Waste Management 121 (2021) 276–285

Contents lists available at ScienceDirect

Waste Management

journal homepage: www.elsevier.com/locate/wasman

Thermochemistry of sulfur during pyrolysis and hydrothermal carbonization of sewage sludges

Rixiang Huang [a,b,*], Yuanzhi Tang [c], Lei Luo [d]

[a] Department of Environmental and Sustainable Engineering, University at Albany, 1400 Washington Ave, Albany, NY 12222, USA
[b] School of Environmental Science and Engineering, Guangzhou University, Guangzhou 510006, China
[c] School of Earth and Atmospheric Sciences, Georgia Institute of Technology, 311 Ferst Dr, Atlanta, GA 30324-0340, USA
[d] State Key Laboratory of Environmental Chemistry and Ecotoxicology, Research Center for Eco-Environmental Sciences, The Chinese Academy of Sciences, Beijing 100085, China

ARTICLE INFO

Article history:
Received 5 August 2020
Revised 19 November 2020
Accepted 1 December 2020
Available online 31 December 2020

Keywords:
Sewage sludge
Sulfur
Heavy metal
Pyrolysis
Hydrothermal carbonization
Chromate adsorption

ABSTRACT

Sulfur (S) is an abundant and redox-active element in urban wastewater systems and plays a critical role in both the wastewater and sludge treatment processes. This study comparatively characterized the transformation of S and several closely associated metals (Cu, Zn, and Fe) during pyrolysis (250 to 750 °C) and hydrothermal carbonization (HTC, 150 to 275 °C) treatments of sewage sludge. S, Fe, Zn, and Cu K-edge X-ray absorption spectroscopy was applied to quantitatively evaluate the fate of S and contribution of different S species in regulating metal speciation. During pyrolysis, aliphatic-S and sulfonate were preferentially degraded at low temperature (below 350 °C) and sulfate was thermochemically reduced at temperature above 450 °C, while metal sulfides (up to 27%) and thiophenes (up to 70%) were increasingly formed. Similar to the pyrolysis process, metal sulfides (up to 40% at temperature above 200 °C) and thiophenes were formed during HTC. The degradation of thiols and organic sulfide, as well as sulfate reduction, released sulfide and strongly affected metal speciation. For example, almost all Cu and half of Zn were transformed into Cu-Fe- or Zn-Fe-sulfides during HTC, whereas they were partially desulfidized during pyrolysis. High abundance of reduced S species (S^{-1} and S^{-2}) in hydrochars may contribute to their strong reductive adsorption of Cr(VI). Results from this work reveal the thermochemical reactions driving the transformations of S and its associated metals during pyrolysis and HTC. The results provide fundamental knowledge for selecting thermochemical sludge treatment techniques for value-added applications of the products.

1. Introduction

Abundant sulfur (S) presents in municipal wastewater and plays a critical role in wastewater and sludge treatment processes, such as corrosion of infrastructure due to H_2S emission (Zhang et al., 2008), speciation modulation of metals (e.g., Cu, Zn, and Ag) (Donner et al., 2011; Kaegi et al., 2011; Lombi et al., 2012), undesirable gas production during biosolids/biogas combustion, and the supplement of S during soil application of biosolids (Luo et al., 2014). Because of these significances, extensive efforts have been devoted to understand and control the flow of S in urban wastewater system and during sludge treatment and application (Fisher et al., 2017; Jiang et al., 2014). S in sewer originates primarily from source water, sulfate salts applied during drinking water treatment, and wastes from human activities (Pikaar et al., 2014). During wastewater treatment process, S is partitioned into the gaseous phase, the treated effluent, and biosolids (Fisher et al., 2017). The removal of S in sewage sludge is generally considered to be primarily via microbial uptake and formation of sulfide precipitates via sulfate reduction (Lens et al., 1998). Therefore, S in wasted activated sludge is primarily constituted by S-containing biomolecules (e.g., amino acids with S-containing side chains), inorganic sulfides, and insoluble sulfate (Dewil et al., 2008; Du and Parker, 2013; Lin et al., 2014).

Sewage sludge is commonly dewatered or anaerobically digested before its final disposal, and the most common disposal options are landfilling, land spreading, and incineration (Kelessidis and Stasinakis, 2012; Lundin et al., 2004; Peccia and Westerhoff, 2015). In recent years, there are growing interests in the application of thermochemical techniques (i.e., carbonization, liquefaction, and gasification) for sewage sludge treatment. These techniques are considered to be more sustainable compared to

* Corresponding author at: Department of Environmental and Sustainable Engineering, University at Albany, 1400 Washington Ave, Albany, NY 12222, USA.
E-mail address: rhuang6@albany.edu (R. Huang).

https://doi.org/10.1016/j.wasman.2020.12.004
0956-053X/

Nomenclature

HTC	Hydrothermal carbonization	EXAFS	Extended X-ray absorption fine structure
AD	Anaerobic digestion	LCF	Linear combination fitting
XAS	X-ray absorption spectroscopy	TT	Target transformation
XANES	X-ray absorption near edge structure		

traditional disposal methods such as landfilling and incineration (Acelas et al., 2014; Wang et al., 2014), as they can target (1) sludge drying and waste reduction (Escala et al., 2013), (2) effective decontamination (of pathogen and organic pollutants) (vom Eyser et al., 2014), (3) fuel production (solid char, oil or syngas) (He et al., 2013; Kim et al., 2014), and (4) functional material production (e.g., sorbent and soil amendment).(Zhang et al., 2013) Thermochemical treatment techniques have been successfully implemented in Japan and many European countries (Christodoulou and Stamatelatou, 2016; Schnell et al., 2020). Pyrolysis and hydrothermal carbonization (HTC) are representative dry and wet thermochemical techniques, respectively, and have been used to convert sludge into solid fuel, sorbent, or soil amendments. HTC is considered to be an energy-efficient treatment option for sludge, because it can accommodate feedstocks with high water content and operates at a relatively low temperature (180 to 280 °C) (Escala et al., 2013; Libra et al., 2011). To optimize these techniques for sludge management, it is important to obtain an in-depth understanding of the transformation of various critical elements embedded in the wastes. In our recent works, we have characterized the transformation of phosphorus (Huang and Tang, 2015, 2016) and abundant heavy metals Cu and Zn (Huang et al., 2018) during the pyrolysis and HTC treatment of sewage sludge. Considering the relevance of S in speciation regulation of elements with strong affinity to S and applications of the treatment products (as solid fuel, sorbent, or soil amendments), it is thus important to study the transformation of S during sewage sludge treatments.

A few recent studies have attempted to characterize S speciation in gaseous, liquid and solid products from both pyrolysis (Liu et al., 2014; Zhang et al., 2017) and HTC (Wang et al., 2020b) of sewage sludge and explore the underlying mechanism. Hydrogen sulfide was identified as the main S species in the gaseous phase and various S-containing organic compounds (e.g., thiols, organic sulfides, and thiophene-S) were identified in the tar during pyrolysis treatment (Zhang et al., 2017). Sulfate is the dominant species identified in the aqueous phase of HTC treatment (Wang et al., 2020b). These studies were able to obtain definite S speciation in the gaseous and liquid products using chromatography, mass spectroscopy or colorimetry. However, solid phase S remains poorly understood, because the few previous studies relied entirely on X-ray photoelectron spectroscopy (XPS) that possesses low S sensitivity and low resolution for S speciation, in addition to being a surface technique (penetration depth is ~10 nm). Moreover, dynamic association between S and metals in the solid phase during pyrolysis or HTC has not been evaluated, impeding in-depth understanding of the thermochemistry of sludge treatment. Speciation information in gaseous and liquid phases may help identify relevant thermochemical reactions responsible for the phase migration of S, but it cannot reveal possible transformation in the solid phase. We recently characterized S species in sludges following hydrothermal hydrolysis (<185 °C, below the normal HTC regime of 180 to 280 °C), and found S was significantly altered at elevated temperature (Wang et al., 2020a).

The objective of this study is thus to fill this knowledge gap and characterize S speciation in solid products from pyrolysis and HTC treatments of activated sludge and anaerobically digested sludge over a broad range of treatment temperatures for a prolonged duration (during which reactions reach steady state). S can exist in a range of organic and inorganic species, some of which can strongly complex with metals such as Cu, Zn, and Fe in sewage sludges, forming corresponding thiol complexes or inorganic sulfides (Donner et al., 2011; Legros et al., 2017). These species may transform during thermochemical treatments and be replaced by more stable species, thus concurrent transformations of these metals were also characterized. Although these metals are stoichiometrically disproportionate to S and may also be complexed by other anions, their speciation can help cross-validate the S speciation results and evaluate its role in regulating metal speciation. In addition, one main application of the produced chars is as a sorbent or soil amendment, the performance of which depends on a range of physicochemical properties of the chars, such as redox reactivity. S is one of the main redox-active elements in sludge and many reduced S species (e.g., thiols and pyrrhotite) are capable of reducing metals such as Cr(VI) (Lay and Levina, 1996; Lu et al., 2006). We thus tested the redox reactivity of the chars using chromate Cr(VI) as a redox active probe. We hypothesize that relative abundance of reduced S species in the chars affects the reductive adsorption of Cr (VI). Results from this work will help gain a deeper insight into the thermochemical mechanisms behind the transformation of various elements in sewage sludge, and provide guidance for treatment optimization and applications of the treatment products.

2. Materials and methods

Sludge samples. The sludges used in this work were collected from F. Wayne Hill wastewater treatment plant (Buford, GA, USA). Specifically, activated sludge was the returning sludge from the secondary clarifier. Anaerobically digested sludge was the final sludge following anaerobic digestion (AD) of primary and secondary sludges, mechanical drying, and mixing of chemical sludge from the ternary treatment. The sludges were stored at −20 °C immediately after sampling, and a portion of them was freeze dried for elemental analysis and pyrolysis treatments. The overall physicochemical properties of the two sludges, such as C, N, P and metals contents, are available in our previous studies (Huang and Tang, 2015, 2016; Huang et al., 2018). S content in the raw sludges and the treated products was analyzed by combustion elemental analyzers (Carlo Erba – Thermo Scientific Costech Instruments).

Thermochemical treatments of sludges. Thermochemical treatments of these sludges followed our previous procedures (Huang and Tang, 2015; Huang et al., 2018). Briefly, pyrolysis of the freeze-dried sludges was carried out using a tube furnace (Thermo Scientific) under argon flow (~1 mL/s) at a range of temperatures (250 to 750 °C), with a heating and cooling rate of 200 °C/h and a soaking duration of 4 h. For each treatment condition, about 1.0 g of the freeze-dried solids was added into an alumina ceramic crucible and inserted into the glass tube. Mass before and after pyrolysis was recorded. The products (hereinafter referred to as pyrochars) were ground into fine powders and stored in tightly sealed vials. HTC was performed using a 20 mL Teflon lined

stainless steel hydrothermal reactor (Parr instrument, IL, USA) or a 100 mL stainless steel high-pressure reactor (Col-INT TECH, SC, USA). For HTC experiments at 150, 175, 200, and 225 °C, wet sludge (12 g, with a solid content of ~10%) was added into the 20 mL Teflon container and mounted in the steel reactor. The reactor was then put into an oven and heated at 150, 175, 200, and 225 °C for 16 h. Due to temperature limit of the 20 mL Teflon lined reactor (<250 °C), reaction at 275 °C was performed in the 100 mL stainless steel reactor with 60 g of sludge and water. At the end of reaction, the reactors were allowed to naturally cool down to room temperature, and the liquid and solid products were separated by centrifugation. The wet solids were freeze-dried and kept in tightly sealed sample vials. The products are referred to as hydrochars. The treatment conditions and sample labels are listed in Table S1. The hydrochars were not washed by organic solvents, because it is unlikely to be practiced at industrial scale and S species in the liquid phase (including oil) are primarily sulfate and sulfide according to a recent study (Wang et al., 2020b).

Chromate adsorption experiment. Selected chars from both pyrolysis and HTC treatments were tested for chromate adsorption. 40 mg finely powdered char samples and 20 mL 0.1 mM K_2CrO_4 in 10 mM KCl were mixed in 50 mL polystyrene centrifuge tubes, and the pH was adjusted to 7.0 using 0.1 M KOH and HCl. The tubes were agitated at 150 rpm at room temperature for 24 h, and the solid and liquid were separated by vacuum filtration (0.45 μm). The filtrate was diluted with 2% HNO_3 for Cr concentration measurement by inductively coupled plasma mass spectrometry (ICP-MS). The wet solids were stored at −20 °C for Cr speciation characterization using XAS.

X-ray absorption spectroscopy (XAS) analysis. Speciation of several closely associated elements (S, Cu, Zn, and Fe) in the raw sludges and chars, as well as Cr in chars following Cr adsorption, was characterized by XAS. S K-edge XANES data were collected at Beamline 4B7A of Beijing Synchrotron Radiation Facility. The finely ground samples were brushed on a conductive double-sided S-free carbon tape, and excess powder was gently blown off. The sample was mounted in an aluminum sample holder and maintained in a vacuum chamber during measurement. Spectra were recorded in fluorescence mode (with an energy range of 2450–2520 eV) with a silicon drift detector (e2v, Chelmsford, UK). The energy was calibrated using Na_2SO_4 with the absorption maximum set at 2482.5 eV. Cu, Zn, Fe, and Cr K-edge XAS data were collected at Beamlines 5BM and 12BM at Advanced Photon Source (APS; Lemont, IL), and Beamline 4–1 and 9–3 at the Stanford Synchrotron Radiation Lightsource (SSRL; Menlo Park, CA). A portion of the Cu and Zn XAS data were collected and reported previously (details in Tables S4 and S5) (Huang et al., 2018). Energy calibration used corresponding metal foils (Cr 5989 eV, Cu 8978.9 eV, Zn 9658.9 eV, Fe 7112.0 eV). Spectra of these metal foils were collected simultaneously during each sample scan for energy reference. Dried sludge and char samples were ground into fine powders and packed with Kapton tape for XAS analysis. XAS data for these samples were collected in fluorescence mode at room temperature using a Vortex detector (APS 5-BM) or multi-element Ge solid-state detectors (APS 12-BM, SSRL BL4-1, and BL9-3). Multiple scans were collected for each sample. A range of reference compounds were prepared for each element and characterized in transmission or fluorescence mode depending on concentration. Details on the reference compounds are described in Table S2. XAS data analysis used the softwares SIXpack and Ifeffit (Ravel and Newville, 2005; Webb, 2005). Multiple scans of each sample were energy calibrated, averaged, background subtracted, and normalized. Principal component analysis (PCA) was conducted on the normalized sample spectra to determine the least number of contributing components, followed by target transformation (TT) to identify candidate reference compounds. S speciation was estimated by linear combination fitting (LCF) of its K-edge XANES data at energy range between 2465 and 2490 eV. The sum of S components was not constrained to 1 during the fitting to evaluate the reliability of the data analysis (Manceau and Nagy, 2012), while the final proportions of the S standards were renormalized to sum to 1. Speciation of Cu was estimated by LCF of its K-edge XANES region (−20 to +100 eV), while that of Zn and Fe was estimated by LCF of their EXAFS region (2.5–11.0 $Å^{-1}$). The TT-determined candidate compounds were used for LCF, and the goodness of fit was determined by R-factor. Fits with the smallest R-factor are reported.

3. Results and discussion

3.1. Compositional difference between two feedstock sludges

Overall, concentrations of S and the studied metals (Cu, Zn, and Fe) are higher in anaerobic sludge than in activated sludge (Huang and Tang, 2015). S content in the activated and anaerobic sludges is respectively 0.78 and 1.21% dry weight (Fig. 1), which falls into the range reported in previous studies (Dewil et al., 2009; Du and Parker, 2013). Fe content is 3.6 and 9.3 wt% in the activated and anaerobic sludges, respectively. Cu and Zn present at a much lower abundance, i.e., ~200 mg/kg and 500 mg/kg in anaerobic sludge, and ~160 mg/kg and 320 mg/kg in activated sludge, respectively (Huang and Tang, 2015). The higher S and metal contents in anaerobic sludge is likely rooted in the sludge source and AD. Anaerobic sludge received primary, activated, and chemical sludge, and organic matter (CHO) is preferentially volatized into biogas during AD, resulting in the enrichment of inorganic species in the sludge.

S speciation in the two sludges was estimated by LCF of the sample spectra using a suite of reference compound spectra. Spectra of the sludges have feature peaks between 2470 eV and 2485 eV (Fig. 2): 1) the peak at ~2473.6 eV suggests the presence of reduced organic S such as thiols, sulfides and thiophenes (oxidation state: −1 and 0), 2) the peak at ~2476.5 eV corresponds to sulfoxide (+2), and 3) the broad peak at 2482.5 eV with a shoulder at ~2481.2 eV is the overlay of sulfonate and sulfate (+5 and +6). LCF results suggest that the identity and relative abundance of the main S species in both sludges and their relative abundance are similar, including thiols, sulfides, and thiophene, sulfonate, and sulfate (Fig. 3 and Table S3). Cu is predominantly sulfidized in both sludges (>90%), although as different sulfide phases (Figs. 4 and S3). Zn is less sulfidized compared to Cu,

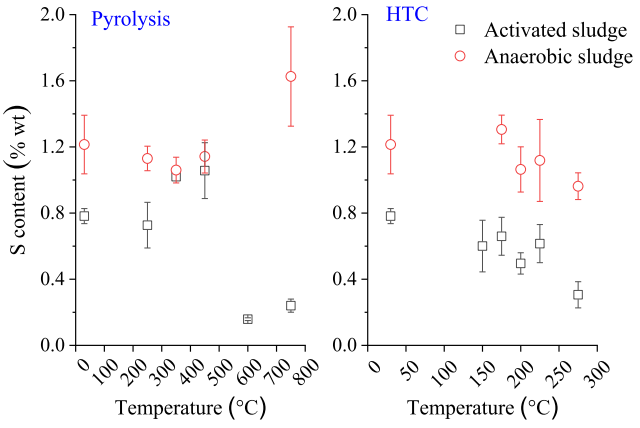

Fig. 1. S content in pyrochars and hydrochars from activated and anaerobically digested sludges. Data points were presented as average ± standard deviation (n = 3 to 6). Raw S content data and S recovery data can be found in Table S1.

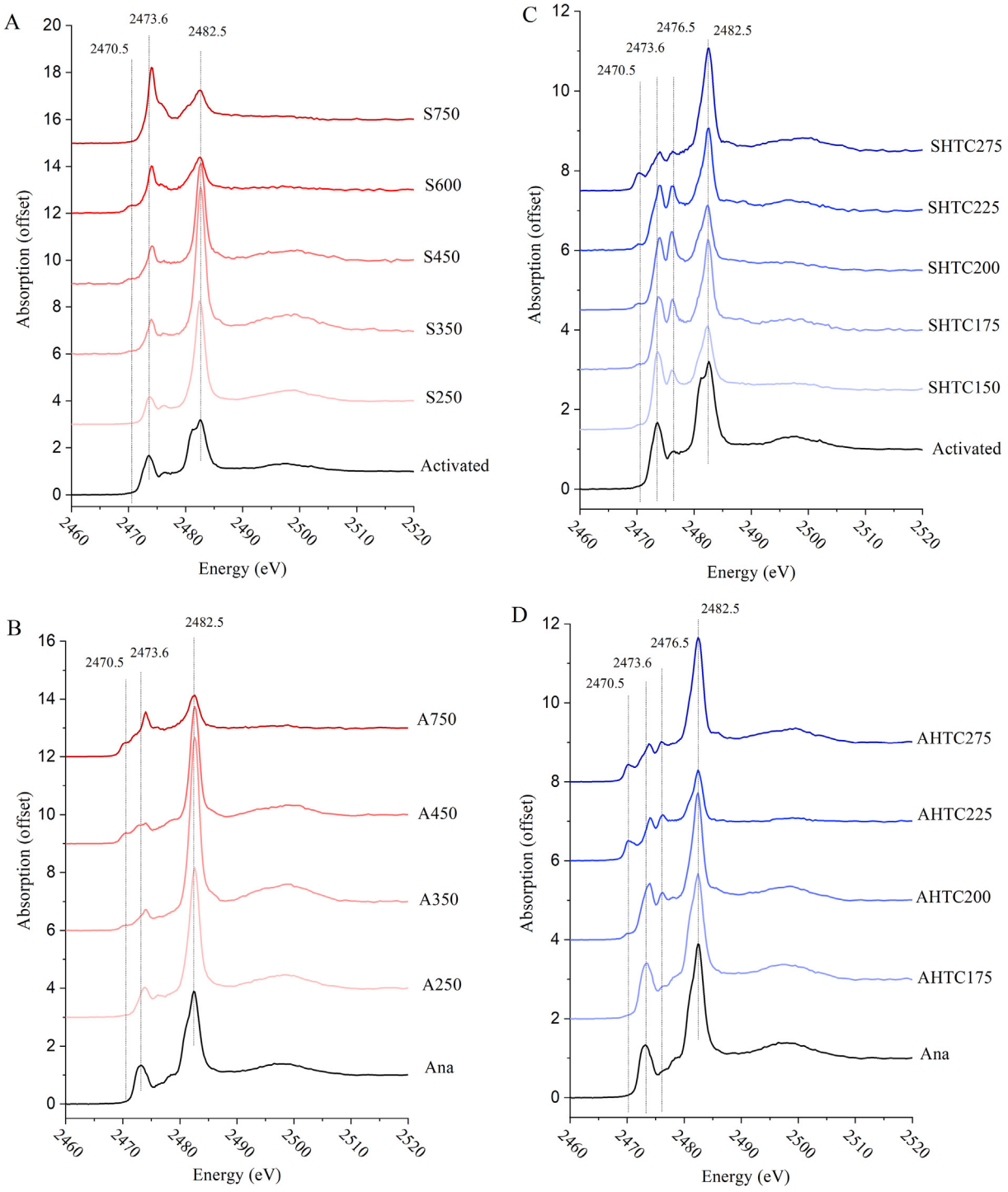

Fig. 2. Normalized S K-edge XANES spectra of activated sludge and its pyrolysis (A) and HTC (C) chars, and anaerobic sludge and its pyrolysis (B) and HTC (D) chars. The vertical dash lines indicate features at the labelled energy, corresponding to white line of specific S compounds (Fig. S1).

and is more sulfidized in anaerobic sludge than in activated sludge (~40 and 75% in activated and anaerobic sludge, respectively) (Figs. S4 and S5). Fe in activated sludge exists primarily as organic complex (51%), Fe(III) phosphate (28%) and oxyhydroxides (13%), while anaerobic sludge consists of primarily Fe(II) species (40% siderite and 20% vivianite) (Fig. 5B). The fact that anaerobic sludge contains more sulfidized Zn and reduced Fe than activated sludge is consistent with the reducing environment during anaerobic digestion process.

3.2. S transformation during pyrolysis and HTC

In general, both activated and anaerobically digested sludges consist of diverse organic and inorganic S species with different thermal stability, and may undergo different transformation pathways. Common organic S structures include mercaptan structure, disulfide, heterocyclic-S, sulfonate, and organosulfate, which are parts of essential biomolecules constituting microbial biomass. Inorganic S includes different metal sulfides and insoluble sulfates,

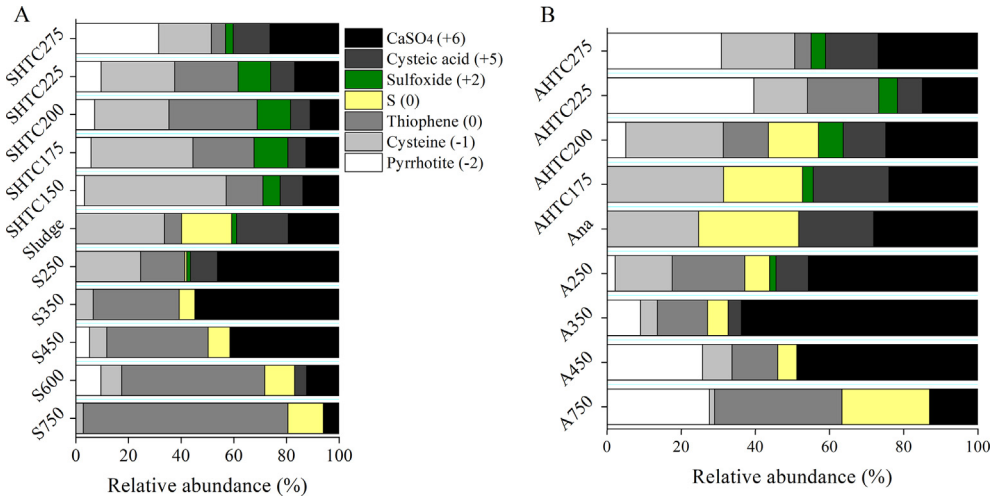

Fig. 3. S speciation of activated sludge and its chars (A) and of anaerobic sludge and its chars (B), estimated by LCF of the S XANES data. The fitted raw data was presented in Table S3. The reference compounds are not exclusive and each may represent various S species with the same valence. $CaSO_4$ includes inorganic and organic sulfate; Cysteic acid represents various sulfonates (R-SO_3H); Sulfoxide represents R-S(O)-R; S(0) represents elemental S; Cysteine includes various thiols (mercaptans), disulfides, and organic sulfides (alkanes or cycloalkanes); Pyrrhotite ($Fe_{(1-x)}S$) represents various metal sulfides.

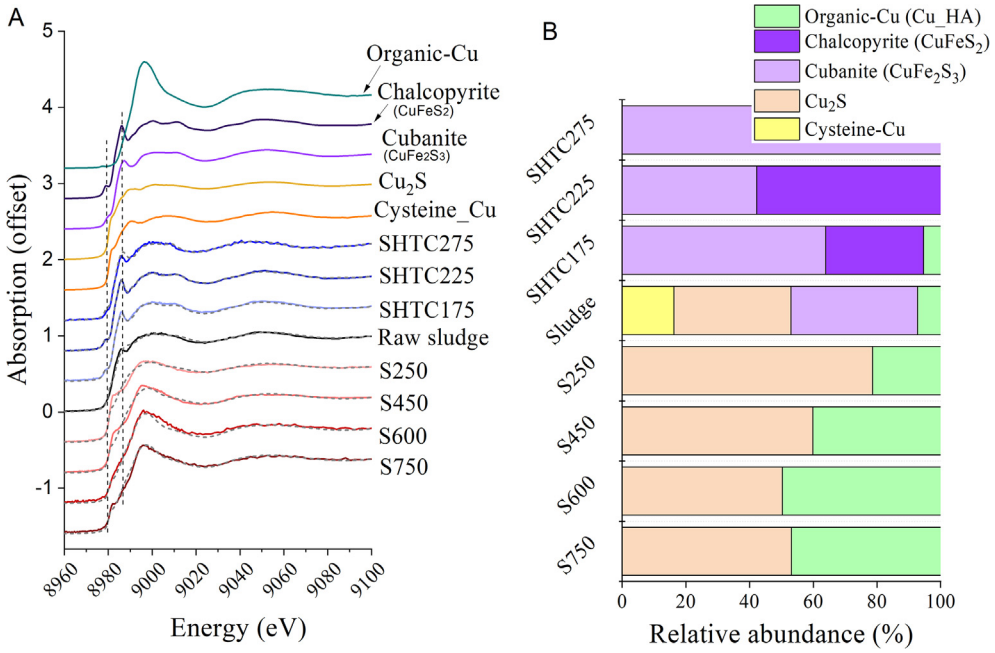

Fig. 4. (A) Cu K-edge XANES spectra of raw activated sludge and its chars, as well as Cu reference compounds. Dash line is the LCF fitting data. (B) Relative abundance of different Cu species estimated from LCF of the XANES data. Vertical dash lines indicate spectral features at 8980 eV and 8986 eV that are characteristics of Cu-Fe sulfides. Spectra and speciation of anaerobic samples are presented in Fig. S3. All fitting raw data is in Table S4.

such as Zn and Cu sulfides, and Ca sulfates. The thermal stability of these S structures and species, and interactions between S and metals during dry and wet thermochemical processes, ultimately control the S volatilization from the solid phase and S speciation in solid products from sewage sludge treatment.

3.2.1. Solid-phase S content and speciation in pyrolysis chars

Solid phase S recovery was calculated from S mass content in the solid chars and total mass recovery of the chars (Table S1 and Fig. 1). The S recovery data showed that S was substantially volatilized (into either the gas and/or oil phases) at elevated pyrolysis temperatures for both sludges, though with different S volatilization behaviors (Table S1). About 36% of S in activated sludge was volatilized from the solid phase after pyrolysis at 250 °C, and the volatilization further decreased slightly at 350 and 450 °C. However, a significant increase in S volatilization occurred at temperature above 600 °C, with only ~10% of S remained in the chars. For anaerobic sludge, although a similar fraction of S was volatilized at 250 °C, S is relatively less volatile at high temperatures, with 41–49% of S remained in the chars.

The XANES spectra showed the following spectral features after pyrolysis treatment (Fig. 2): 1) sharpening and enhancement of the peak at 2482.5 eV between 250 °C and 450 °C; 2) appearance and gradual increase of a small peak at ~2470.5 eV at elevated temperatures, and 3) shifting of the peak at ~2473.6 eV to higher energies. At temperature below 350 °C, the relative decrease in peak intensity at 2473.6 eV as well as enhancement of the peak at 2482.5 eV and weakening of the shoulder peak correspond respectively to the

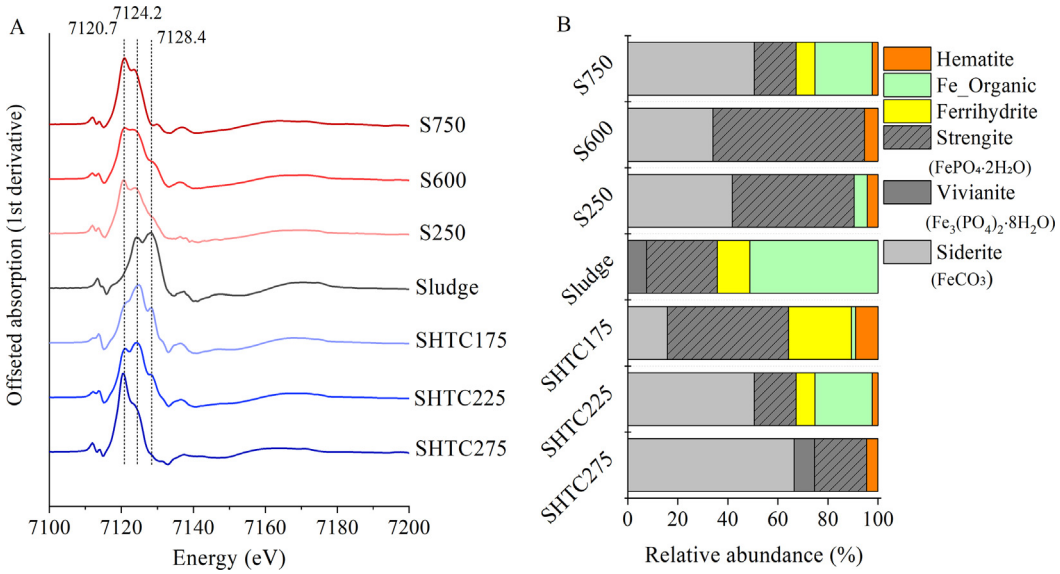

Fig. 5. (A) First derivative of Fe K-edge XANES spectra for activated sludge and its chars, and (B) Fe speciation estimated by LCF of the K-edge EXAFS spectra. The vertical dash lines indicate features at 7120.7, 7124.2, and 7128.4 eV, respectively. Normalized XANES spectra and LCF of the EXAFS spectra can be found in Fig. S6. Data for anaerobic samples are presented in Fig. S7. All fitting raw data is in Table S6.

decrease of aliphatic-S species (such as thiols and organic sulfides, fitted as cysteine) and sulfonates, as well as increase of sulfate abundance in the chars (Fig. 3). Previous studies showed that gaseous production of H_2S was fast and aliphatic-S in tar was abundant at temperature below 500 °C (Zhang et al., 2017). This suggests the preferential fragmentation and volatilization of aliphatic-S species, as well as oxidation of sulfonate into sulfate. At temperature above 350 °C, shifting of the peak at ~2473.6 eV to higher energy and decrease of the peak intensity at 2482.5 eV correspond to the increasing abundance of thiophene (white line peaks at 2474 eV) and decreasing abundance of sulfate. In addition, abundant metal sulfides (fitted as pyrrhotite) were formed, especially in chars from anaerobic sludge. At this temperature range, sulfate is reduced and thiophene is formed from other S species, and the formation of metal sulfides contributes to S retention in the solid phase.

Comparatively, more thiophene is formed in chars from activated sludge, while more metal sulfides were formed in chars from anaerobic sludge. Speciation difference between the two sludge-derived chars at temperature above 350 °C is consistent with the difference in S volatilization behavior between the two raw sludges, which is likely caused by the difference in composition and potential to form stable S-containing species at high temperature. Thiophenes are generally polymerized from thiols or organic sulfides (Amrani, 2014), which are more abundant in the activated sludge than in anaerobic sludge (34% vs 24%) because anaerobic sludge has experienced extensive hydrolysis and microbial degradation of the organic matter. Therefore, activated sludge has more organic-S species to be polymerized, while anaerobic sludge contains more Fe and chalcophile metals (i.e., Cu and Zn) to form metal sulfides.

3.2.2. Solid-phase S content and speciation in HTC chars

S content in hydrochars of both sludges gradually decreased as HTC temperature increased, and the trend was similar between the two sludges (Fig. 1, Table S1). Because of the higher S content in pristine anaerobic sludge and its higher mass recovery compared to activated sludge, less S was lost from the solid phase (via solubilization or volatilization) during HTC of anaerobic sludge (32–56% for anaerobic sludge compared to 54–62% for activated sludge).

Comparison of the S XANES spectra of the hydrochar samples reveals the following spectral changes (Fig. 2C and D): (1) appearance and gradual increase of the peak at 2470.5 eV suggests the formation of metal sulfides, (2) shifting of the peak at ~2473.6 eV to 2474 eV indicates an increase of thiophene abundance, and (3) enhanced intensity of the peak at 2476.5 eV up to 225 °C correlates to the formation of sulfoxide. The first two changes were similar to the changes observed for pyrolysis. During HTC of activated sludge, relative abundance of thiophene and sulfoxide increases as HTC temperature increases (up to 225 °C), and abundance of metal sulfides increases over the whole temperature range (Fig. 3). Compared to that of activated sludge, the relative abundance of thiophene and sulfoxide during HTC of anaerobic sludge is much smaller, and more metal sulfides formed. Compared to the pyrolysis process, aliphatic-S is more persistent during HTC, along with the abundant metal sulfides, resulting in overall more reduced S in HTC chars.

3.3. Speciation transformation of Cu, Zn and Fe

LCF of the XAS data of Cu and Zn showed that Cu existed primarily as cysteine complex, chalcocite, and cubanite (Figs. 4 and S3B), and Zn as wurtzite, hopeite, and ferrihydrite-associated Zn, in raw sludges (Fig. S5). Compared to Cu and Zn, limited Fe was associated with S based on LCF of Fe XAS. Fe exists primarily as organic complexes, oxyhydroxides, and phosphates in raw sludges, with more Fe (II) species in anaerobic sludge than those in activated sludge (62.5% vs 7.5%) (Figs. 5 and S7D).

3.3.1. Speciation transformation during pyrolysis

After pyrolysis treatment, the relative abundance of Cu and Zn sulfides decreased at elevated pyrolysis temperatures, with those in activated sludge being less stable (Figs. 4and S5A). For Cu, more organic complex was formed, likely from the degradation of organic sulfides. For Zn, the Zn sulfide was degraded and replaced by Fe mineral associated Zn (Fig. S5). Following pyrolysis treatment, Fe was significantly reduced, as evidenced in shifting of the spectra to lower energies at increasing treatment temperatures

(Figs. 5A and S7). The reduction was most significant in the treatment of activated sludge, because most Fe in anaerobic sludge already existed in reduced form. Following pyrolysis at 250 to 750 °C, the portion of Fe(II) increased from 7.5% to about 35–50%, existing dominantly as siderite (Fig. 5B). Desulfurization of Cu and Zn phases was consistent with the degradation of thiols and organic sulfides during pyrolysis.

3.3.2. Speciation transformation during HTC

After HTC treatment, Cu transformed from diverse sulfide species into Cu-Fe sulfides (cubanite and chalcophile) at temperature from 175 to 275 °C (Fig. 4B). In comparison, no significant change in Zn sulfide abundance was observed at temperature up to 225 °C, while most Zn sulfide was degraded at temperature above 225 °C (Fig. S5). The formation of chalcopyrite and their persistence under hydrothermal conditions are consistent with the results of S XANES that metal sulfides (in the form of pyrrhotite) formed under the same conditions. Similar to pyrolysis, Fe was reduced after HTC (Fig. 5A). Transformation of Fe was more temperature dependent during HTC than during pyrolysis, with siderite abundance increases from 16% °C at 175 to 75% at 275 °C (Figs. 5B and S7D).

The lack of Fe sulfides such as pyrite, pyrrhotite, and troilite in the Fe LCF result is likely due to their relatively low abundance among all Fe species (as only <30% of total S are metal sulfides, and S content is much lower than that of Fe). For example, in the sample (AHTC225) with maximum metal sulfide abundance (~40% of the 1 wt% of S) based on S XANES data, even assuming all of the sulfides were a single Fe sulfide species it only accounts for a maximum of ~3–4% of the total Fe (20 wt%) in the sample. This small value, in combination with the generally accepted ~10% error range for LCF of XAS, explained the absence of Fe sulfide species in the LCF of Fe XANES. However, the increase in Fe reduction during both treatments was consistent with the trends of S, Cu, and Zn transformations, in that sulfate was reduced during pyrolysis and Cu- and Zn-Fe sulfides (i.e., chalcopyrite and wurtzite) formed under HTC conditions.

3.4. Redox reactivity of the chars using chromate as a probe

S is a highly redox-active element, and its speciation transformation is expected to affect the redox property of the treatment products. In this study, we use chromate adsorption as a probe to evaluate the reductive reactivity of the chars. Reduced S species (e.g., thiols and pyrrhotite) are known to be capable of reducing chromate (Lay and Levina, 1996; Lu et al., 2006) and these species were identified in our char products. Results of chromate adsorption showed that pyrochars and hydrochars possess different chromate adsorption capacity and involves different adsorption mechanisms (Fig. 6). Overall, hydrochars adsorbed more chromate (~1000 mg/kg) than pyrochars (<200 mg/kg), and pyrochars derived from anaerobic sludge adsorbed more chromate than those from activated sludge at the same temperature (Fig. 6A). Chromate was completely reduced to Cr(III) following adsorption on hydrochars, while not all chromate adsorbed by pyrochars was reduced, particularly for those from activated sludge (Fig. 6B). The reduction of Cr(VI) into Cr(III) that may form highly insoluble phosphate, sulfate, or hydroxide precipitates (phosphate and sulfate are abundant in the chars and can be water soluble), are likely responsible for the enhanced removal of chromate from the aqueous phase. Despite the limited chromate amount adsorbed, about 30% of the total Cr remained as Cr(VI) on pyrochars derived from activated sludge. The results suggest that chromate adsorption was primarily driven by reductive adsorption, and the observed variation in adsorption abilities was closely associated with S speciation. For example, the relative abundance of reduced S species (fitted as cysteine and pyrrhotite) was much higher in hydrochars than in pyrochars, and that in pyrochars from anaerobic sludge was higher than pyrochars from activated sludge. Although a few studies have shown the ability of sludge-derived pyrochars to adsorb chromate, the adsorption mechanisms were not revealed (Chen et al., 2015; Zhang et al., 2013). Our results provide direct evidence for the reductive adsorption mechanism and show the relevance of S. It is worthy to note that other reduced species such as non-S organic compounds and Fe (II) species may also contribute to chromate reduction, thus more systematic studies on Cr adsorption isotherms and S transformation following Cr adsorption are needed to quantify the contribution of specific S species.

3.5. Thermochemistry of S transformation

Pyrolysis is a dry thermochemical process, during which organic structures undergo complex reactions such as fragmentation, depolymerization and aromatization. S K-edge XANES data showed a preferential decrease of aliphatic-S (i.e., mercaptan, organic sulfides, and disulfides) in pyrochars during low T pyrolysis, which agrees with the preferential release of gaseous H_2S and aliphatic-S compounds in tar shown by a previous study (Zhang et al., 2017). Therefore, aliphatic-S is preferentially fragmented, contributing to significant S volatilization from the solid phase. The preferential loss of aliphatic-S, along with sulfonate oxidation, results in the predominance of sulfate in low temperature pyrochars. At higher temperature range (>350 °C), S transformation seems to be driven by two main processes: thermochemical reduction of sulfate and aromatization. Thiophene is increasingly formed in both the solid and tar phases at temperature above 350 °C, as demonstrated in our S K-edge XANES data and previous analysis of tar composition (Zhang et al., 2017). Decrease in sulfate abundance is caused by thermochemical sulfate reduction, during which sulfate is reduced into sulfide by organic compounds (Watanabe et al., 2009; Wei et al., 2012). The formation of pyrrhotite ($Fe_{1-x}S$, likely include other more reduced sulfide species) is most likely from the formation and reduction of pyrite (FeS_2), which is an intermediate of Fe reduction by H_2S. This phenomenon has been observed in the pyrolysis of pyrite-rich kerogen (Kelemen et al., 2010). Because compared to activated sludge, anaerobic sludge consists of higher contents of metals, such as Ca, Fe, and chalcophiles, formation of metal sulfides is likely to contribute to higher S retention in its pyrochars.

There are similarities and differences between the HTC and pyrolysis processes. The similarities are the formation of thiophene and metal sulfides, although their temperature dependency is different. Opposite to the results of pyrolysis, relative abundance of thiophene did not increase monotonically and relative abundance of metal sulfides increased monotonically with temperature during HTC treatment. In addition, compared to rapid degradation of thiols and sulfonate during pyrolysis, these two species were relatively persistent over the HTC temperature range. Metal sulfides were increasingly formed, likely a result of metal complexation with inorganic sulfides solubilized from organic structures, as evidenced in Cu speciation result that organic Cu sulfides were displaced with Cu-Fe sulfides. Difference in S thermochemistry between pyrolysis and HTC can be attributed to factors such as temperature range, water, and reaction environment, which control the types and rate of reactions occurred. HTC is a close and relatively homogeneous system that all products (e.g., H_2S) remain in the system and involved in subsequent reactions, such as the formation of inorganic sulfides. In comparison, pyrolysis operates at a higher temperature range and is a semi-open system (where gaseous and liquid products are separated from the solid phases after forming). Pyrolysis at high temperature is conducive to aromatization and polymerization of organic structures, thus forming more thiophenes than HTC (Fig. 3). Main reactions driving the above-

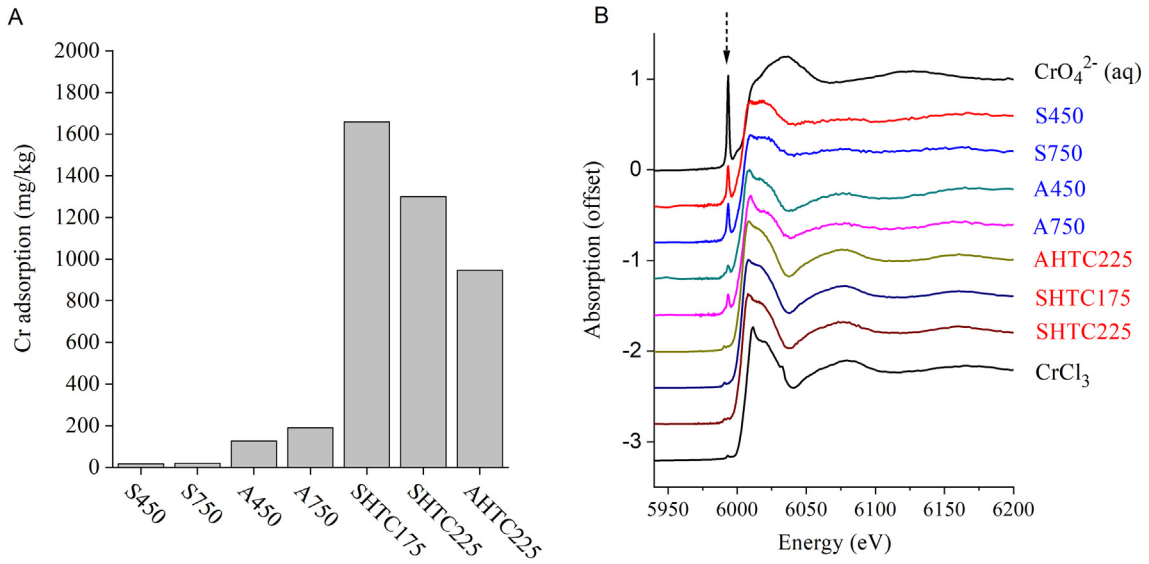

Fig. 6. (A) Cr adsorption amount onto selected pyrochars and hydrochars and (B) Cr K-edge XANES spectra of adsorption samples and Cr(III) and Cr(VI) references. Arrow indicates the pre-edge feature for Cr(VI).

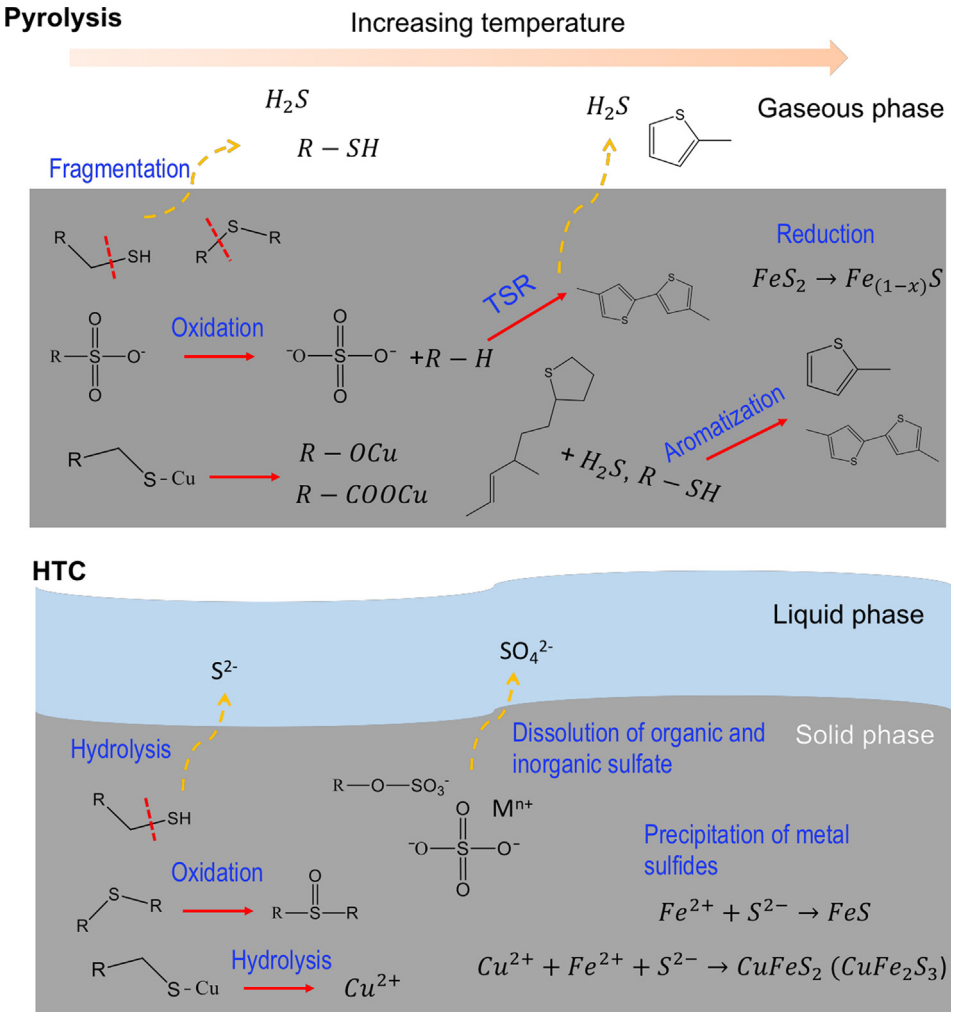

Fig. 7. Schematic illustration of main thermochemical reactions underlying S speciation transformation during pyrolysis and HTC treatments of sewage sludges. TSR – thermochemical sulfate reduction. The volatilization/solubilization of S species were based on previous results (Wang et al., 2020b; Zhang et al., 2017).

mentioned transformation during pyrolysis and HTC were summarized in Fig. 7.

Although S accounts for only a small mass fraction of sludges and the treatment products, it plays a key role in modulating the properties and functionalities of sludge treatment products because of its redox-active nature. Speciation of S is fundamental to its role, because of its diverse oxidation states and redox couples (Jocelyn, 1967; Mirzahosseini and Noszal, 2016). Our results showed that pyrolysis and HTC significantly transform S in sewage sludges, affecting not only the speciation of chalcophile metals, but also the reducing ability of the produced chars, as evidenced in the reductive adsorption of chromate.

4. Conclusions

Thermochemical transformation of S during pyrolysis and HTC treatments of activated and anaerobic sludges over a range of temperatures was explored, by characterizing speciation of S and three closely associated metals in the treatment products. Degradation of aliphatic-S species such as thiols and organic sulfides and oxidation of sulfonate are the main reactions at low temperature pyrolysis (250–450 °C), and thermochemical sulfate reduction and aromatization are the main processes at high temperature range (450–750 °C). HTC shares some similar trends as pyrolysis, such as the formation of thiophene and metals sulfides, while also differs by the formation of sulfoxides and persistence of aliphatic-S. Speciation of Cu, Zn, and Fe complementarily substantiates the changes of metal sulfides during the treatment. Metal contents in the pristine sludges were found to affect the extent of S retention and metal sulfide formation in the solid phase, as shown in the difference between activated and anaerobic sludges. Different impacts of pyrolysis and HTC on S speciation seem to contribute to their difference in redox activity, as demonstrated by the different reductive adsorption abilities for chromate by the chars. Because targeted value-added applications of the thermochemical treatment products are soil amendment and sorbent, mechanistic understanding of S transformation and its impacts gained in this work can provide scientific basis for developing sludge treatment and product application strategies.

Associated content

Flow diagram of the studied WWTP and sampling sites; Details of pyrolysis and HTC treatment conditions and sample information; mass recovery and S content; K-edge XANES or EXAFS spectra for S, Cu, Zn, and Fe; LCF results for the K-edge XAS data.

Declaration of Competing Interest

The authors declare that they have no known competing financial interests or personal relationships that could have appeared to influence the work reported in this paper.

Acknowledgement

This work is supported by National Science Foundation grant #1739884 and National Natural Science Foundation of China (41703091). We thank Robert Harris (F. Wayne Hill Water Resources Center) for sludge sample collection and Dr. Ellery Ingall for assistance in S content analysis. We also appreciate the support from beamline scientists Ryan Davis, Matthew Latimer and Erik Nelson at Beamline 4-1 and 9-3, Qing Ma at APS Beamline 5-BM-D, and many others at beamline 4B7A of Beijing Synchrotron Radiation Facility. Portions of this research were conducted at the Advanced Photon Source (APS) and Stanford Synchrotron Radiation Lightsource (SSRL). APS is a U.S. Department of Energy (DOE) Office of Science User Facility operated for the DOE Office of Science by Argonne National Laboratory under Contract No. DE-AC02-06CH11357. Use of SSRL, SLAC National Accelerator Laboratory, is supported by DOE Office of Science, Office of Basic Energy Sciences under Contract No. DE-AC02-76SF00515.

Appendix A. Supplementary material

Supplementary data to this article can be found online at https://doi.org/10.1016/j.wasman.2020.12.004.

References

Acelas, N.Y., López, D.P., Brilman, D.W., Kersten, S.R., Kootstra, A.M.J., 2014. Supercritical water gasification of sewage sludge: gas production and phosphorus recovery. Bioresour. Technol. 174, 167–175.
Amrani, A., 2014. Organosulfur Compounds: Molecular and Isotopic Evolution from Biota to Oil and Gas. Annu. Rev. Earth Planet. Sci. 42 (1), 733–768.
Chen, T., Zhou, Z., Xu, S., Wang, H., Lu, W., 2015. Adsorption behavior comparison of trivalent and hexavalent chromium on biochar derived from municipal sludge. Bioresour. Technol. 190, 388–394.
Christodoulou, A., Stamatelatou, K., 2016. Overview of legislation on sewage sludge management in developed countries worldwide. Water Sci. Technol. 73 (3), 453–462.
Dewil, R., Baeyens, J., Roels, J., Steene, B.V.D., 2008. Distribution of sulphur compounds in sewage sludge treatment. Environ. Eng. Sci. 25 (6), 879–886.
Dewil, R., Baeyens, J., Roels, J., Van De Steene, B., 2009. Evolution of the total sulphur content in full-scale wastewater sludge treatment. Environ. Eng. Sci. 26 (4), 867–872.
Donner, E., Howard, D.L., Jonge, M.D.D., Paterson, D., Cheah, M.H., Naidu, R., Lombi, E., 2011. X-ray Absorption and Micro X-ray Fluorescence Spectroscopy Investigation of Copper and Zinc Speciation in Biosolids. Environ. Sci. Technol. 45 (17), 7249–7257.
Du, W.W., Parker, W., 2013. Characterization of Sulfur in Raw and Anaerobically Digested Municipal Wastewater Treatment Sludges. Water Environ. Res. 85 (2), 124–132.
Escala, M., Zumbühl, T., Koller, C., Junge, R., Krebs, R., 2013. Hydrothermal carbonization as an energy-efficient alternative to established drying technologies for sewage sludge: A feasibility study on a laboratory scale. Energy Fuels 27 (1), 454–460.
Fisher, R.M., Alvarez-Gaitan, J.P., Stuetz, R.M., Moore, S.J., 2017. Sulfur flows and biosolids processing: Using Material Flux Analysis (MFA) principles at wastewater treatment plants. J. Environ. Manage. 198, Part 1, 153–162.
He, C., Giannis, A., Wang, J.Y., 2013. Conversion of sewage sludge to clean solid fuel using hydrothermal carbonization: Hydrochar fuel characteristics and combustion behavior. Appl. Energy 111, 257–266.
Huang, R., Tang, Y., 2015. Speciation Dynamics of Phosphorus during (Hydro) Thermal Treatments of Sewage Sludge. Environ. Sci. Technol. 49 (24), 14466–14474.
Huang, R., Tang, Y., 2016. Evolution of phosphorus complexation and mineralogy during (hydro)thermal treatments of activated and anaerobically digested sludge: Insights from sequential extraction and P K-edge XANES. Water Res. 100, 439–447.
Huang, R., Zhang, B., Saad, E.M., Ingall, E.D., Tang, Y., 2018. Speciation evolution of zinc and copper during pyrolysis and hydrothermal carbonization treatments of sewage sludges. Water Res. 132, 260–269.
Jiang, G., Wightman, E., Donose, B.C., Yuan, Z., Bond, P.L., Keller, J., 2014. The role of iron in sulfide induced corrosion of sewer concrete. Water Res. 49, 166–174.
Jocelyn, P., 1967. The standard redox potential of cysteine-cystine from the thiol-disulphide exchange reaction with glutathione and lipoic acid. Eur. J. Biochem. 2 (3), 327–331.
Kaegi, R., Voegelin, A., Sinnet, B., Zuleeg, S., Hagendorfer, H., Burkhardt, M., Siegrist, H., 2011. Behavior of Metallic Silver Nanoparticles in a Pilot Wastewater Treatment Plant. Environ. Sci. Technol. 45 (9), 3902–3908.
Kelemen, S.R., Walters, C.C., Kwiatek, P.J., Freund, H., Afeworki, M., Sansone, M., Lamberti, W.A., Pottorf, R.J., Machel, H.G., Peters, K.E., Bolin, T., 2010. Characterization of solid bitumens originating from thermal chemical alteration and thermochemical sulfate reduction. Geochim. Cosmochim. Acta 74 (18), 5305–5332.
Kelessidis, A., Stasinakis, A.S., 2012. Comparative study of the methods used for treatment and final disposal of sewage sludge in European countries. Waste Manage. 32 (6), 1186–1195.
Kim, D., Lee, K., Park, K.Y., 2014. Hydrothermal carbonization of anaerobically digested sludge for solid fuel production and energy recovery. Fuel 130, 120–125.
Lay, P.A., Levina, A., 1996. Kinetics and mechanism of chromium(VI) reduction to chromium(III) by L-cysteine in neutral aqueous solutions. Inorg. Chem. 35 (26), 7709–7717.
Legros, S., Levard, C., Marcato-Romain, C.E., Guiresse, M., Doelsch, E., 2017. Anaerobic digestion alters copper and zinc speciation. Environ. Sci. Technol. 51 (18), 10326–10334.

Lens, P.N.L., Visser, A., Janssen, A.J.H., Pol, L.W.H., Lettinga, G., 1998. Biotechnological Treatment of Sulfate-Rich Wastewaters. Crit. Rev. Environ. Sci. Technol. 28 (1), 41–88.
Libra, J.A., Ro, K.S., Kammann, C., Funke, A., Berge, N.D., Neubauer, Y., Titirici, M.-M., Fühner, C., Bens, O., Kern, J., Emmerich, K.-H., 2011. Hydrothermal carbonization of biomass residuals: a comparative review of the chemistry, processes and applications of wet and dry pyrolysis. Biofuels 2 (1), 71–106.
Lin, H., Ye, C., Lv, L., Zheng, C.R., Zhang, S., Zheng, L., Zhao, Y., Yu, X., 2014. Characterization of extracellular polymeric substances in the biofilms of typical bacteria by the sulfur K-edge XANES spectroscopy. J. Environ. Sci. 26 (8), 1763–1768.
Liu, H., Zhang, Q., Hu, H.Y., Xiao, R.X., Li, A.J., Qiao, Y., Yao, H., Naruse, I., 2014. Dual role of conditioner CaO in product distributions and sulfur transformation during sewage sludge pyrolysis. Fuel 134, 514–520.
Lombi, E., Donner, E., Tavakkoli, E., Turney, T.W., Naidu, R., Miller, B.W., Scheckel, K. G., 2012. Fate of zinc oxide nanoparticles during anaerobic digestion of wastewater and post-treatment processing of sewage sludge. Environ. Sci. Technol. 46 (16), 9089–9096.
Lu, A.H., Zhong, S.J., Chen, J., Shi, J.X., Tang, J.L., Lu, X.Y., 2006. Removal of Cr(VI) and Cr(III) from aqueous solutions and industrial wastewaters by natural clino-pyrrhotite. Environ. Sci. Technol. 40 (9), 3064–3069.
Lundin, M., Olofsson, M., Pettersson, G.J., Zetterlund, H., 2004. Environmental and economic assessment of sewage sludge handling options. Resour. Conserv. Recycl. 41 (4), 255–278.
Luo, L., Xu, C., Ma, Y., Zheng, L., Liu, L., Lv, J., Zhang, S., 2014. Sulfur speciation in an arable soil as affected by sample pretreatments and sewage sludge application. Soil Sci. Soc. Am. J. 78 (5), 1615–1623.
Manceau, A., Nagy, K.L., 2012. Quantitative analysis of sulfur functional groups in natural organic matter by XANES spectroscopy. Geochim. Cosmochim. Acta 99, 206–223.
Mirzahosseini, A., Noszal, B., 2016. Species-specific standard redox potential of thiol-disulfide systems: A key parameter to develop agents against oxidative stress. Sci. Rep. 6.
Peccia, J., Westerhoff, P., 2015. We should expect more out of our sewage sludge. Environ. Sci. Technol. 49 (14), 8271–8276.
Pikaar, I., Sharma, K.R., Hu, S.H., Gernjak, W., Keller, J., Yuan, Z.G., 2014. Reducing sewer corrosion through integrated urban water management. Science 345 (6198), 812–814.
Ravel, B., Newville, M., 2005. ATHENA, ARTEMIS, HEPHAESTUS: data analysis for X-ray absorption spectroscopy using IFEFFIT. J. Synchrotron Radiat. 12 (4), 537–541.
Schnell, M., Horst, T., Quicker, P., 2020. Thermal treatment of sewage sludge in Germany: A review. J. Environ. Manage. 263, 110367.
vom Eyser, C., Palmu, K., Otterpohl, R., Schmidt, T.C., Tuerk, J., 2014. Determination of pharmaceuticals in sewage sludge and biochar from hydrothermal carbonization using different quantification approaches and matrix effect studies. Anal. Bioanal. Chem., 1–10
Wang, L.P., Zhang, L., Li, A.M., 2014. Hydrothermal treatment coupled with mechanical expression at increased temperature for excess sludge dewatering: Influence of operating conditions and the process energetics. Water Res. 65, 85–97.
Wang, Q., Zhang, C., Patel, D., Jung, H., Liu, P., Wan, B., Pavlostathis, S.G., Tang, Y., 2020a. Coevolution of iron, phosphorus, and sulfur speciation during anaerobic digestion with hydrothermal pretreatment of sewage sludge. Environ. Sci. Technol. 54 (13), 8362–8372.
Wang, Z., Zhai, Y., Wang, T., Peng, C., Li, S., Wang, B., Liu, X., Li, C., 2020b. Effect of temperature on the sulfur fate during hydrothermal carbonization of sewage sludge. Environ. Pollut. 260, 114067.
Watanabe, Y., Farquhar, J., Ohmoto, H., 2009. Anomalous fractionations of sulfur isotopes during thermochemical sulfate reduction. Science 324 (5925), 370–373.
Webb, S., 2005. (2005) SIXpack: a graphical user interface for XAS analysis using IFEFFIT. Phys. Scr. T115, 1011.
Wei, Z., Walters, C.C., Michael Moldowan, J., Mankiewicz, P.J., Pottorf, R.J., Xiao, Y., Maze, W., Nguyen, P.T.H., Madincea, M.E., Phan, N.T., Peters, K.E., 2012. Thiadiamondoids as proxies for the extent of thermochemical sulfate reduction. Org. Geochem. 44, 53–70.
Zhang, J., Zuo, W., Tian, Y., Chen, L., Yin, L., Zhang, J., 2017. Sulfur transformation during microwave and conventional pyrolysis of sewage sludge. Environ. Sci. Technol. 51 (1), 709–717.
Zhang, L., De Schryver, P., De Gusseme, B., De Muynck, W., Boon, N., Verstraete, W., 2008. Chemical and biological technologies for hydrogen sulfide emission control in sewer systems: A review. Water Res. 42 (1), 1–12.
Zhang, W., Mao, S., Chen, H., Huang, L., Qiu, R., 2013. Pb(II) and Cr(VI) sorption by biochars pyrolyzed from the municipal wastewater sludge under different heating conditions. Bioresour. Technol. 147, 545–552.